

Tissue-Penetrating Delivery of Compounds and Nanoparticles into Tumors

Kazuki N. Sugahara,^{1,5} Tambet Teesalu,^{1,5} Priya Prakash Karmali,² Venkata Ramana Kotamraju,¹ Lilach Agemy,¹ Olivier M. Girard,³ Douglas Hanahan,⁴ Robert F. Mattrey,³ and Erkki Ruoslahti^{1,2,*}

¹Vascular Mapping Center, Burnham Institute for Medical Research at UCSB, Biology II Building, University of California, Santa Barbara, Santa Barbara, CA 93106-9610, USA

²Cancer Research Center, Burnham Institute for Medical Research, 10901 North Torrey Pines Road, La Jolla, CA 92037, USA

³Department of Radiology, University of California, San Diego, 408 Dickinson Street, San Diego, CA 92103-8226, USA

⁴Department of Biochemistry and Biophysics, Diabetes and Comprehensive Cancer Centers, University of California, San Francisco, 513 Parnassus Avenue, San Francisco, CA 94143, USA

⁵These authors contributed equally to this work

*Correspondence: ruoslahti@burnham.org

DOI 10.1016/j.ccr.2009.10.013

SUMMARY

Poor penetration of drugs into tumors is a major obstacle in tumor treatment. We describe a strategy for peptide-mediated delivery of compounds deep into the tumor parenchyma that uses a tumor-homing peptide, iRGD (CRGDK/RGPD/EC). Intravenously injected compounds coupled to iRGD bound to tumor vessels and spread into the extravascular tumor parenchyma, whereas conventional RGD peptides only delivered the cargo to the blood vessels. iRGD homes to tumors through a three-step process: the RGD motif mediates binding to α_v integrins on tumor endothelium and a proteolytic cleavage then exposes a binding motif for neuropilin-1, which mediates penetration into tissue and cells. Conjugation to iRGD significantly improved the sensitivity of tumor-imaging agents and enhanced the activity of an antitumor drug.

INTRODUCTION

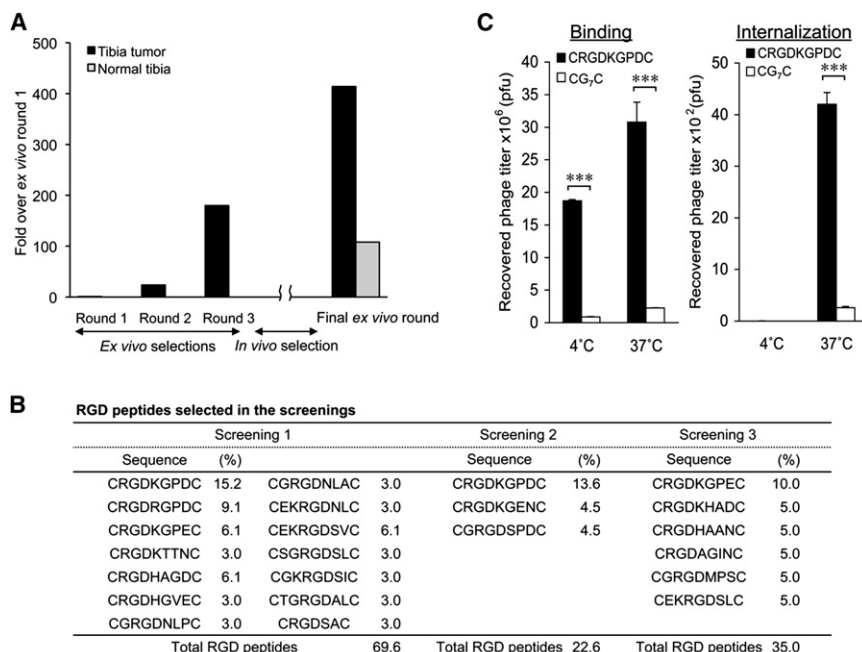
The vasculature in different tissues expresses distinct biochemical signatures, the “vascular zip codes” (Ruoslahti, 2002; Ruoslahti and Rajotte, 2000). Vascular zip codes can serve as targets for docking-based (synaptic) delivery of diagnostics and therapeutics. α_v integrins are highly expressed in tumor vasculature, where they can be accessed with peptides containing the RGD integrin recognition motif (Eliceiri and Cheresh, 2001; Pierschbacher and Ruoslahti, 1984; Ruoslahti, 2002, 2003). RGD-based synaptic targeting has been successfully used to deliver drugs, biologicals (Arap et al., 1998; Curnis et al., 2004), imaging agents (Sipkins et al., 1998), viruses (Pasqualini et al., 1997; Wickham, 2000), and nanoparticles (Murphy et al., 2008) to tumor vasculature. However, crossing the vascular wall and penetrating into the tumor parenchyma against the elevated interstitial pressure in tumors remains a major challenge in tumor therapy (Heldin et al., 2004; Jain, 1990).

We have recently identified a consensus R/KXXR/K motif as a mediator of cell and tissue penetration (Teesalu et al., 2009). The receptor for the R/KXXR/K motif was shown to be neuropilin-1. This motif is not active unless it occupies a C-terminal position in the peptide; we refer to this position effect as the C-end Rule (CendR).

The interaction between the CendR motif and neuropilin-1 appears to be a key determinant for penetration of biological barriers. For example, vascular endothelial growth factor-165 and certain semaphorins bind to neuropilin-1 through C-terminal CendR motifs and thereby increase vascular permeability (Acevedo et al., 2008; Jia et al., 2006; Soker et al., 1998; Teesalu et al., 2009). In addition, many viruses possess CendR motifs within their capsid proteins and often require proteolytic cleavage to expose the CendR motif to be infective, a process that requires penetration of biological barriers (Steinhauer, 1999; Teesalu et al., 2009). One such virus, HTLV-1, has been shown to use its CendR motif (KPXR) to bind to and internalize

SIGNIFICANCE

Targeted delivery of compounds to tumor vessels and tumor cells can enhance tumor detection and therapy. Docking-based (synaptic) targeting strategies use peptides, antibodies, and other molecules that bind to tumor vessels and tumor cells to deliver more drug to tumors than to normal tissues. A major obstacle to applying this principle has been the limited transport of the targeted payload into tumor parenchyma. The iRGD peptide we describe here overcomes this limitation and establishes a capability for tissue-penetrating drug delivery.

**Figure 1. Identification of iRGD Peptide**

(A) A representative example of the enrichment obtained in phage library screens on prostate cancer bone metastases. Three screens with similar results were performed.

(B) RGD peptides selected in the screens. Approximately 50 individual clones were randomly picked for sequencing from phage pools recovered in the final round of ex vivo phage display. Clones that gave unsuccessful sequencing results were omitted during the analysis. The proportion of each RGD peptide is shown.

(C) Binding and internalization to PPC1 human prostate cancer cells of phage expressing the CRGDKGPDC peptide. PPC1 cells were incubated with phage displaying CRGDKGPDC or a polyglycine control peptide CG₇C for 1 hr at 4°C or 37°C. To assess internalization, phage bound at the cell surface was removed by washing the cells with an acid buffer. Note that the internalization of CRGDKGPDC phage occurs at 37°C but not at 4°C. Statistical analysis was performed with Student's t test. n = 3; error bars, SEM; ***p < 0.001.

into immune cells in a neuropilin-1-dependent fashion to infect the cells (Lambert et al., 2009).

We hypothesized that the tissue-penetrating properties of the CendR system could be used to deliver drugs and nanoparticles into tumor parenchyma, beyond the vascular barrier. Here we report results obtained with a peptide that combines tumor-homing and CendR-dependent tissue-penetrating properties. We also evaluate the potential of the technology for clinical applications by performing magnetic resonance imaging (MRI) and tumor treatment studies.

RESULTS

Identification of iRGD

We used a cyclic CX₇C (C, cysteine; X, any amino acid) peptide library displayed on T7 phage (diversity approximately 10⁹; Hoffman et al., 2003) to identify peptides that recognize tumor blood vessels in experimental metastasis mouse models of human prostate cancer (see Figure S1 available online). Three rounds of ex vivo phage display selection with cell suspensions from bone tumors were followed by one in vivo selection for homing to the bone tumors (Hoffman et al., 2003). The resulting phage pools bound to tumor-derived cell suspensions 200–400 times more than the original library, and the binding to the tumor cell suspensions was five times higher than to cell suspensions from normal bone (Figure 1A). Individual phage clones were randomly picked from the phage pools and sequenced. Phage that contained the RGD motif (Pierschbacher and Ruoslahti, 1984; Ruoslahti, 2003) within three related sequences, CRGDKGPDC, CRGDRGPDC, and CRGDKGPEC, dominated in the selected pools (Figure 1B). CRGDKGPDC, which was most frequent, bound to cultured PPC1 human prostate cancer cells at 4°C, appeared to internalize into them at 37°C (Figure 1C), and was named “iRGD” (internalizing RGD).

Homing of iRGD to Tumors

We synthesized a fluorescein-labeled iRGD (FAM-iRGD) and intravenously injected the peptide into tumor-bearing mice. FAM-iRGD accumulated in tumor tissue in every model we tested. These include orthotopic xenografts of prostate, pancreatic ductal, and breast cancer; bone and brain xenografts of prostate carcinoma; and genetically engineered models of de novo pancreatic neuroendocrine (islet), pancreatic ductal, and cervical cancer (summarized in Table S1). The tumors, but not normal tissues, were strongly fluorescent under UV light (Figure 2A and Figure S2). Confocal microscopy revealed accumulation of FAM-iRGD peptide in and around tumor vessels and in tumor parenchyma (Figure 2B), but not in normal tissues (Figure S3). Remarkably, iRGD phage (diameter about 65 nm; Sokoloff et al., 2000) and a synthetic iRGD-coated nanoparticle, self-assembling micelles (diameter 15–25 nm; Arleth et al., 2005; Karmali et al., 2009), also reached extravascular tumor parenchyma (Figures 2B). Two conventional RGD peptides and their corresponding peptide-displaying phage, CRGDC and RGD-4C, which both have strong affinities for α v integrins (Koivunen et al., 1993, 1995), also homed to tumors, but accumulated only in and around tumor blood vessels and did not disperse throughout the interstitium like iRGD (Figure 2B). Quantification of the area of peptide homing further demonstrated that iRGD homes to and spreads within the tumor tissue far more efficiently than CRGDC (Figure 2C). The difference in the distribution of payloads linked to iRGD and other RGD peptides was even more pronounced when a genetically engineered model of de novo pancreatic ductal adenocarcinoma (PDAC; Hezel et al., 2006) with an extensive amount of interstitium was used as the target (Figure S4). Whole-body imaging of PDAC mice injected with FAM-iRGD micelles labeled with the near-infrared dye Cy7 produced a strong and specific signal in the tumors, illustrating the potential of iRGD for tumor targeting (Figure S5).

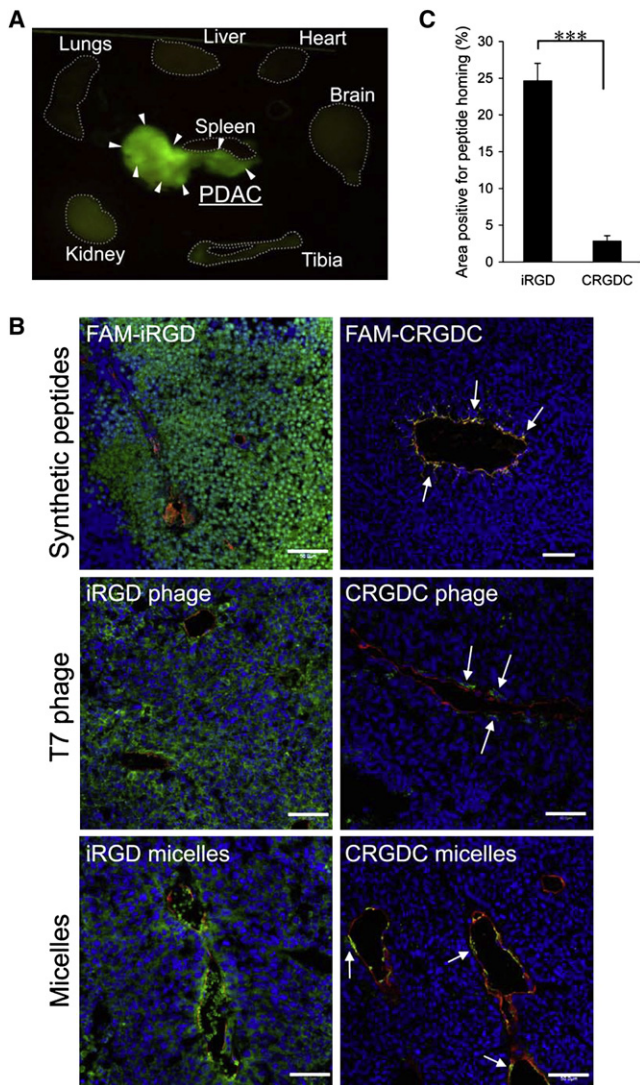


Figure 2. In Vivo Tumor Homing of iRGD Peptide
(A) Approximately 200 μ g of FAM-iRGD or control peptide in PBS was intravenously injected into *Kras^{G12D}, p48-Cre, Ink4a^{+/-}* mice bearing de novo PDAC. The peptides were allowed to circulate for 2 hr and organs were collected and viewed under UV light. Arrowheads point to the tumors. Dotted lines show where the organs were placed. Representative images from four experiments are shown.
(B) Confocal images of orthotopic 22Rv1 human prostate cancer xenografts from mice injected with the indicated peptides, phage, and micelles. iRGD was compared to a similar integrin-binding but nonpenetrating peptide, CRDGC. The circulation time was 2 hr for the free peptides, 15 min for the phage, and 3 hr for the micelles. Red, CD31; green, peptides, phage, or micelles; blue, nuclei. Arrows point to CRGDC compounds in or just outside the vessel walls, illustrating its homing to the tumor vasculature. Representative fields from multiple sections of five tumors are shown. Scale bars, 50 μ m.
(C) Quantification of tumor homing area of iRGD and CRGDC peptides. Cryosections of 22Rv1 orthotopic tumors from mice injected with FAM-iRGD or FAM-CRGDC peptide were immunohistochemically stained with an anti-FITC antibody. The samples were subjected to image analysis with Scanscope CM-1 scanner for quantification of the FAM-positive areas. Statistical analysis was performed with Student's t test. n = 3; error bars, SEM; ***p < 0.001.

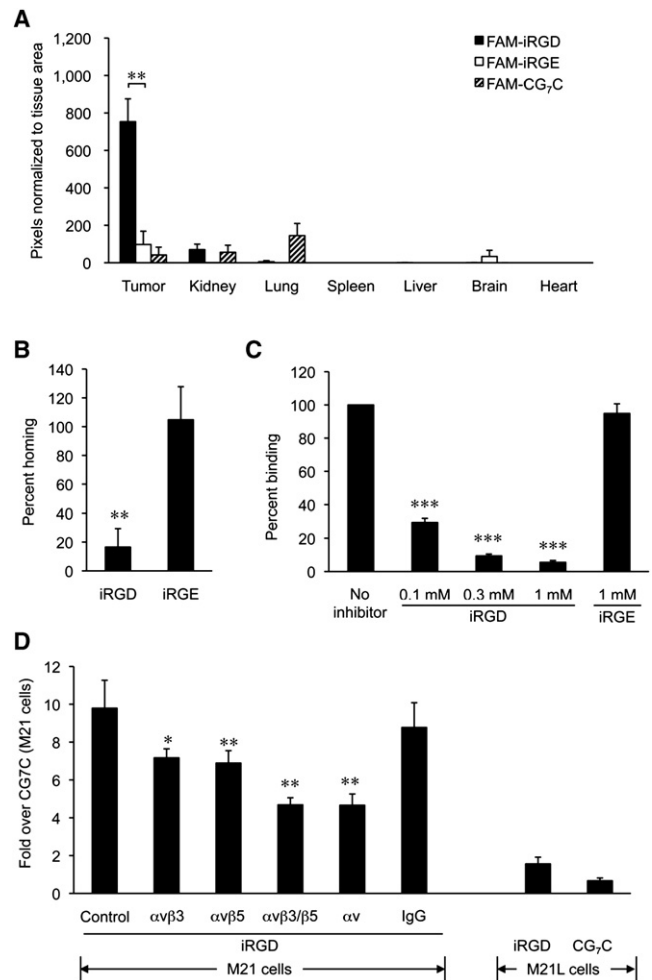


Figure 3. iRGD Binds to α v Integrins

(A) Quantification of the in vivo distribution of iRGD and control peptides. FAM-iRGD; a non-integrin-binding iRGD mutant, FAM-CRG(E)KGPDC (FAM-iRGE); and a FAM-labeled cyclic polyglycine control peptide, FAM-CG₇C, were injected into PDAC mice as described in Figure 2A. Fluorescence in each tissue was quantified with Image J.
(B) Inhibition of the tumor homing of FAM-iRGD with nonlabeled iRGD. A 10-fold excess of unlabeled iRGD peptide or iRGE peptide was injected 30 min before the injection of FAM-iRGD in PDAC mice. Fluorescence was quantified as above. FAM-iRGD homing without injection of unlabeled peptide was considered as 100%.
(C) Dose-dependent inhibition of iRGD phage binding to PPC1 prostate cancer cells by synthetic iRGD peptide and iRGE. iRGD phage binding without inhibitors was considered as 100%.
(D) Inhibition of iRGD phage binding to α v integrin expressing M21 cells by antibodies against integrins or control mouse IgG (left panel). Lack of iRGD phage binding to M21 cells selected for low level of α v integrin expression (M21L; right panel). Statistical analyses were performed with Student's t test in (A) and (B) and with ANOVA in (C) and (D). n = 3; error bars, SEM; *p < 0.05; **p < 0.01; ***p < 0.001.

Integrin-Dependent Binding of iRGD to Tumor Cells

The in vivo homing of iRGD to tumors is dependent on the RGD motif. Control peptides including a nonintegrin binding variant (Pierschbacher and Ruoslahti, 1984; Ruoslahti, 2003), CRGEKGPDC (iRGE), produced minimal tumor fluorescence (Figure 3A). Coinjecting an excess of unlabeled iRGD peptide

reduced the accumulation of FAM-iRGD in tumors, whereas iRGE peptide did not have such an effect (Figure 3B). The *in vitro* binding of iRGD to cancer cells also required the RGD motif because the binding of iRGD phage to PPC1 cells at 4°C was inhibited dose dependently by free iRGD peptide, but not by iRGE (Figure 3C).

The RGD-directed integrins $\alpha v\beta 3$, $\alpha v\beta 5$, and $\alpha 5\beta 1$ are upregulated in angiogenic endothelial cells and certain tumor cells (Eliceiri and Cheresh, 2001; Ruoslahti, 2002). PPC1 cells express $\alpha v\beta 5$ and $\alpha 5\beta 1$, but not $\alpha v\beta 3$ (Figure S6A). An anti- $\alpha v\beta 5$ antibody almost completely inhibited iRGD phage binding to PPC1 cells, whereas inhibitory antibodies against $\alpha 5\beta 1$ and other integrins had no effect (Figure S6B). M21 human melanoma cells (Cheresh and Spiro, 1987; Figure S7) expressing both $\alpha v\beta 3$ and $\alpha v\beta 5$ integrins bound iRGD phage, whereas variants lacking expression of these integrins did not, confirming the αv integrin dependency of iRGD binding (Figure 3D). The binding of the iRGD phage was reduced by both anti- $\alpha v\beta 3$ or anti- $\alpha v\beta 5$ (Figure 3D), indicating that iRGD recognizes both of these integrins.

The binding affinity of synthetic iRGD peptide to purified $\alpha v\beta 3$ integrin was $K_d = 17.8 \pm 8.6$ nM and $K_d = 61.7 \pm 13.3$ nM to $\alpha v\beta 5$ integrin (Table S2). The affinities of two previously identified cyclic RGD peptides, RGD-4C and CRGDC (Koivunen et al., 1993, 1995), for $\alpha v\beta 3$ and $\alpha v\beta 5$ were also in the same range, as shown by measuring the ability of each peptide to block iRGD binding (Table S2). Thus, differences in integrin-binding specificity or affinity do not explain the distinct ability of iRGD from the other two RGD peptides to penetrate tumor cells and tissue. Rather, the evidence implicates a second motif in iRGD, dubbed the CendR motif, in this capability.

iRGD as a CendR Peptide

iRGD contains a cryptic CendR motif, RGDK/R, and possesses CendR-like tissue and cell-penetrating activities (Teesalu et al., 2009). However, the CendR motif in iRGD is not C-terminal, which is a prerequisite for CendR activity (Teesalu et al., 2009). Therefore, we hypothesized that iRGD, having been recruited to cell surfaces through the RGD-integrin interactions, is proteolytically processed and that the processing generates a C-terminal RGDK/R sequence capable of binding to neuropilin-1 (schematized in Figure 4).

To investigate this proteolysis hypothesis, we first examined whether iRGD binds to PPC1 cells in a CendR-dependent manner after being treated by a protease to expose a C-terminal arginine or lysine; PPC1 cells have substantial levels of neuropilin-1 expression (Teesalu et al., 2009). Because the protease(s) that we postulate to cleave iRGD is unknown, we chose to use trypsin for this purpose, as its specificity predicts that it would produce a derivative iRGD peptide with the requisite C-terminal arginine or lysine. As shown in Figure 5A, trypsin treatment of iRGD phage enhanced the binding of iRGD phage to PPC1 cells to a level comparable to a prototypic CendR peptide, RPARPAR (Teesalu et al., 2009). Trypsin had no effect on phage expressing CRGDC (Figure 5A) or RGD-4C (data not shown). The binding at 4°C of the trypsin-treated iRGD phage was blocked by UV-treated noninfectious phage expressing RPARPAR, but not by phage displaying a peptide in which the CendR motif was disrupted by addition of an alanine residue to the C terminus (RPARPARA; Teesalu et al., 2009). The binding of intact iRGD phage

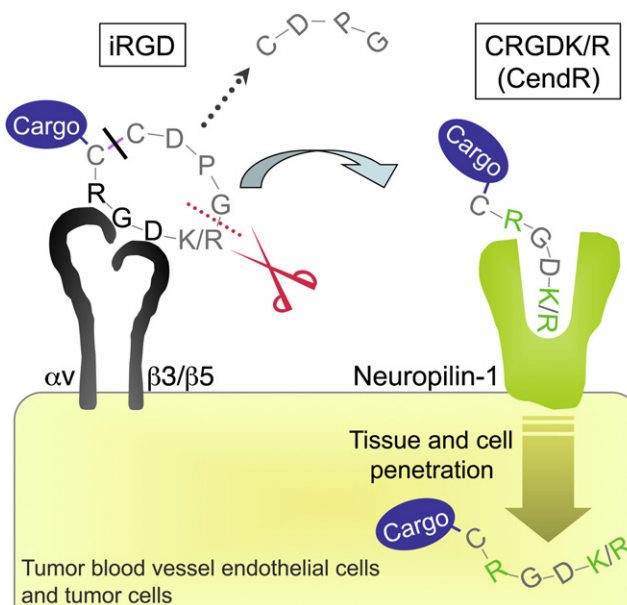


Figure 4. Multistep Binding and Penetration Mechanism of iRGD

The iRGD peptide accumulates at the surface of αv integrin-expressing endothelial and other cells in tumors. The RGD motif mediates the integrin binding. The peptide is cleaved by a cell surface-associated protease(s) to expose the cryptic CendR element, RXXX/R, at the C terminus (red dotted line). The CendR element then mediates binding to neuropilin-1, with resulting penetration of cells and tissues. The peptide can penetrate into tumor cells and tissues with a cargo, such as a simple chemical or a nanoparticle, provided that the cargo is attached to the N terminus of the iRGD peptide because the disulfide bond apparently breaks before the peptide is internalized (black line).

was not affected by RPARPAR (data not shown), supporting our hypothesis that iRGD does not exhibit CendR features unless its CendR motif is activated by exposure at the C terminus.

To determine whether the CendR motif in iRGD is indeed activated by cellular proteases, we incubated FAM-iRGD that carries the fluorophore at its N terminus with PPC1 prostate cancer cells and isolated intracellular products by affinity chromatography on anti-FITC (FAM) antibodies. To prevent cytoplasmic proteolysis, while allowing proteolysis at the cell surface, the incubation was done in the presence of a proteasome inhibitor. We detected no intracellular full-length FAM-iRGD, but recovered the FAM-CRGDK fragment (Figure S8). When iRGD with FAM on its C terminus was used, no intracellular iRGD fragment was recovered (data not shown). These results show that CRGDK, the N-terminal half of iRGD with a C-terminal CendR motif, is the cell-penetrating fragment of iRGD, as postulated in Figure 4.

Prompted by the results indicating that proteolytically released CRGDK is the active cell-penetrating component of iRGD, we engineered phage expressing CRGDK and found that it bound to and penetrated into PPC1 cells. The binding of the CRGDK phage was inhibited by CRGDK peptide, indicating a specific binding (Figure 5B). The binding process was also inhibited by the RPARPAR peptide, which has a C-terminal arginine, but not by RPARPARA (Figure 5B). Antibodies against various integrins, including αv integrins, had no effect on the CRGDK binding, indicating that the binding is CendR dependent and does not

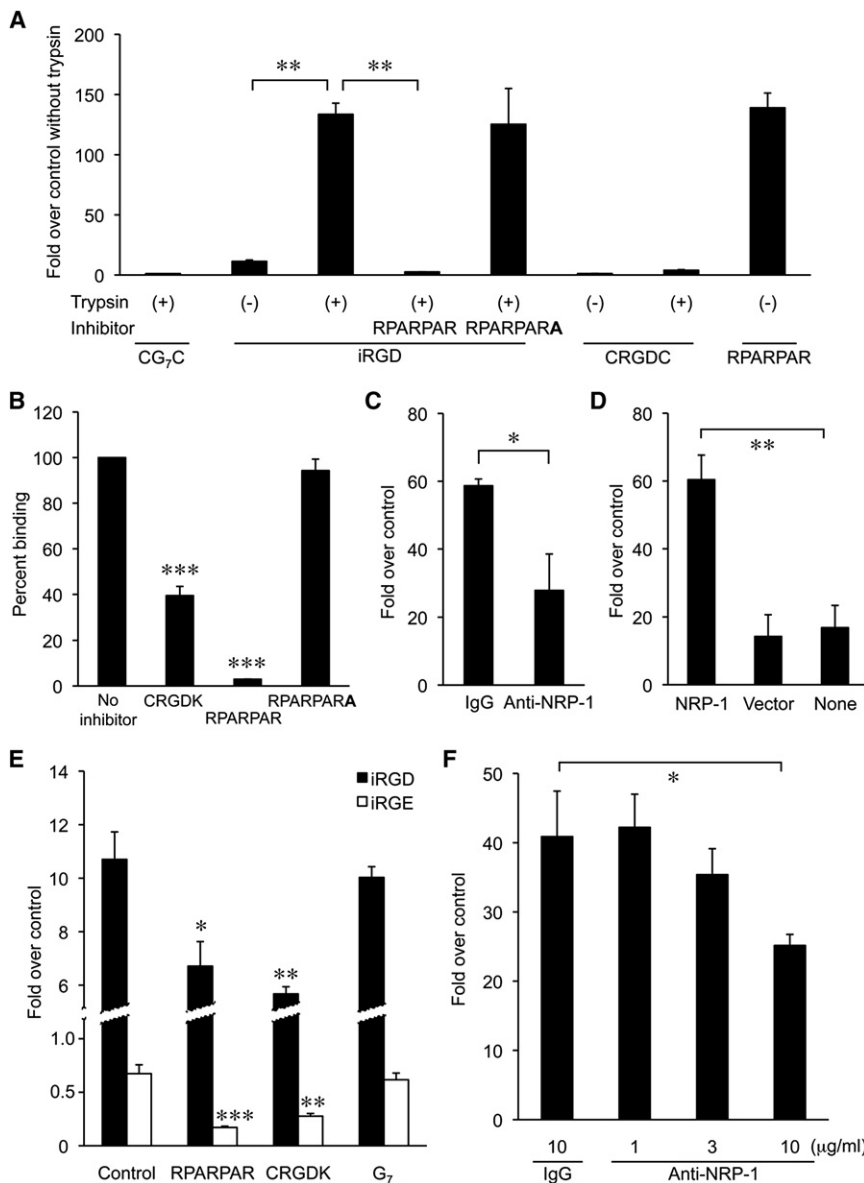


Figure 5. CendR Motif in iRGD Penetration of Tumor Cells

(A) The penetration of trypsin-treated iRGD phage within PPC1 cells pretreated or not with noninfectious RPARPAR or RPARPAR(A) phage. (B) Inhibition of CRGDK phage binding to PPC1 by synthetic CRGDK, RPARPAR, and RPARPAR(A) peptides. CRGDK phage binding without inhibitors was considered as 100%. (C) CRGDK phage binding to PPC1 cells treated with anti-neuropilin-1 blocking antibodies (anti-NRP-1) or control goat IgG. (D) CRGDK phage binding to M21 cells transfected with neuropilin-1 cDNA to induce forced expression of neuropilin-1 (NRP-1), vector alone, or without transfection. (E) Inhibition of iRGD and iRGE phage penetration into PPC1 by noninfectious phage displaying the CendR peptides RPARPAR and CRGDK. (F) Dose-dependent inhibition of iRGD phage penetration of PPC1 cells by anti-neuropilin-1 antibodies (anti-NRP-1) to block neuropilin-1 function. Statistical analyses were performed with ANOVA in (A), (B), and (E) and Student's t test in (C), (D), and (F). $n = 3$; error bars, SEM; * $p < 0.05$; ** $p < 0.01$; *** $p < 0.001$.

involve integrins (data not shown). Moreover, an antibody against neuropilin-1, the receptor for CendR peptides (Teesalu et al., 2009), reduced the binding (Figure 5C). CRGDK phage did not substantially bind to or penetrate into M21 cells, which express only minimal amounts of neuropilin-1 (Figure S9). However, forced expression of neuropilin-1 in these cells (Teesalu et al., 2009) increased the binding (Figure 5D) and penetration (data not shown) approximately 3.5 fold. Affinity measurements revealed that the CRGDK peptide binds to neuropilin-1 with a K_d ($1.4 \pm 0.6 \mu\text{M}$; Table S2) similar to that of RPARPAR ($K_d = 1.7 \pm 0.2 \mu\text{M}$; Teesalu et al., 2009). These results indicate that CRGDK binds to cells and penetrates into them using the CendR pathway.

In keeping with the possibility that the RGD CendR element is the cell-penetrating sequence in iRGD, both CRGDK and RPARPAR UV-treated phage inhibited iRGD phage penetration into PPC1 cells at 37°C (Figure 5E). Anti-neuropilin-1 also inhibited

the penetration of iRGD phage (Figure 5F), but had little effect on binding of iRGD phage to PPC1 cells at 4°C (data not shown). We further tested the relative roles of the RGD and RXXK motifs in iRGD by using the iRGE phage, which does not bind to integrins due to the disrupted RGD motif (Pierschbacher and Ruoslahti, 1984; Ruoslahti, 2003), but still contains a CendR motif, RXXK. The iRGE phage did penetrate PPC1 cells at 37°C, and both RPARPAR and CRGDK inhibited the penetration (Figure 5E), implicating the CendR pathway. The penetration was less effective than that of iRGD, presumably because iRGE lacks integrin

binding that would concentrate the phage at the cell surface. These results indicate that iRGD penetrates cells through the CendR pathway using the RXXK sequence and that the penetration is likely facilitated by initial binding to integrins through RGD.

Confocal microscopy showed that iRGD phage and neuropilin-1 colocalized in cultured cells (Figure S10), supporting the involvement of the neuropilin-1-dependent CendR pathway in the tumor cell penetration by iRGD. Phage displaying an iRGD variant that lacks the CendR motif (CRGDGGPDC) or the two other conventional RGD peptides, CRGDC and RGD-4C, did not colocalize with neuropilin-1, nor did they penetrate the cells efficiently.

Neuropilin-1-Dependent Penetration of iRGD within Tumor Tissue

We next investigated the neuropilin-1 dependence of in vivo tissue penetration by iRGD into PDAC. Preinjection of tumor-bearing mice with a function-blocking anti-neuropilin-1 antibody

inhibited the penetration of iRGD phage in tumor tissue. The phage were trapped in the tumor blood vessels or stayed in close association with the vessels (Figure 6A, right panel). Preinjection of control IgG did not affect the spreading of iRGD (Figure 6A, left panel). Phage expressing the iRGD variant that lacks the CendR motif but retains RGD (CRGDGGPDC) targeted tumor blood vessels, but did not spread into tumor tissue (data not shown).

Studies on the time dependence of iRGD homing and penetration further supported the importance of αv integrin and neuropilin-1 expression in this process. FAM-iRGD peptide injected intravenously into mice bearing PDAC tumors initially colocalized with tumor blood vessels, which were positive for both αv integrins and neuropilin-1 (Figure 6B, top panels, arrows). The peptide subsequently extravasated, presumably because it induces increased permeability in tumor vessels (Teesalu et al., 2009), and gradually appeared within tumor cells in ductal structures (Figure 6B, middle panels). Most of the tumor cells were positive for αv integrins (Figure 6B, left panels). Importantly, tumor cells strongly positive for neuropilin-1 were particularly effective at accumulating and retaining FAM-iRGD (Figure 6B, right panels). Similar results were obtained in an orthotopic prostate cancer xenograft model; the iRGD peptide also homed to areas that overexpress both αv integrins and neuropilin-1 in these tumors. The human 22Rv1 prostate cancer cells used in the model express αv integrins and neuropilin-1 on the cell surface (Figures S11A and S11B).

iRGD in Tumor Imaging and Treatment

To investigate the potential of iRGD for clinical applications, we performed MRI and therapeutic targeting experiments. For MRI, mice bearing 22Rv1 orthotopic xenografts were injected intravenously with iRGD peptide-linked superparamagnetic iron oxide nanoworms (about 80 nm long and 30 nm thick; Park et al., 2009; Simberg et al., 2007). Iron oxide nanoparticles are evidenced as hypointensities in T2-weighted magnetic resonance images (McAteer et al., 2007). In addition to hypointense vascular signals, the iRGD nanoworms gave low intensity regions that spread throughout the tumor, while CRGDC nanoworms only decreased the intensity of the tumor vasculature (Figure 7, T2-weighted magnetic resonance images). Untargeted nanoworms produced no detectable signal under identical imaging conditions. Confocal microscopy of the tumors confirmed the enhanced tissue penetration of the iRGD nanoworms (Figure 7, rightmost panels). Both the MRI results and optical imaging (Figure S5) indicate that iRGD is capable of delivering diagnostics to tumors and that tumors are more efficiently visualized with this peptide than with conventional RGD peptides.

The ability of iRGD to deliver anticancer drugs was investigated by treating mice bearing orthotopic 22Rv1 tumors with iRGD-coated abraxane, a 130 nm nanoparticle consisting of albumin-embedded paclitaxel (Haley and Frenkel, 2008; Karmali et al., 2009). In vitro, iRGD-abraxane inhibited the proliferation of 22Rv1 cells more efficiently than abraxane conjugated with a cyclic RGD peptide without a CendR motif (CRGDC; Koivunen et al., 1993) or abraxane alone (Figure S12A). Intravenously injected iRGD-abraxane spread more within tumor tissue than the other abraxane formulations (Figures S12B). Quantification of the drug showed that 8-fold more abraxane accumulated in the tumors from injections of iRGD-abraxane than of nontargeted

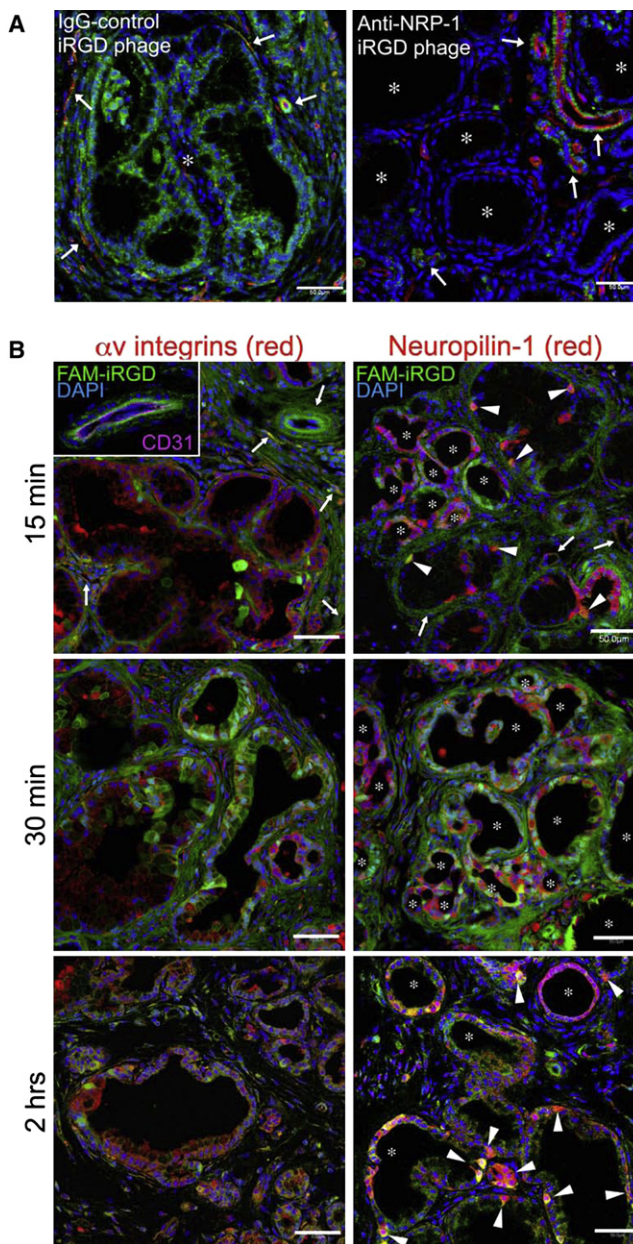


Figure 6. Penetration of iRGD within Tumor Tissue Involves Neuropilin-1

(A) Neuropilin-1-dependent spreading of iRGD phage within tumor tissue. Confocal images of PDAC tumors from transgenic mice preinjected with a function-blocking anti-neuropilin-1 antibody (anti-NRP-1) or an IgG-control, followed by injection with the iRGD phage. Green, phage; red, CD31; blue, DAPI. Arrows and asterisks represent blood vessels and tumor ducts, respectively. Representative images from three independent sets of studies are shown. Scale bars, 50 μ m.

(B) Time-dependent homing of FAM-iRGD peptide (green) in relation to the expression of αv integrins (red, left panels) and neuropilin-1 (red, right panels) in PDACs. The blood vessels targeted by FAM-iRGD were positive for both αv integrins and neuropilin-1 (arrows). The inset shows CD31 staining (magenta) of a blood vessel targeted by FAM-iRGD. Nearly all tumor ducts examined were positive for αv integrins. Tumor cells (arrowheads) and tumor ducts (asterisks) also strongly positive for neuropilin-1 were particularly effective in internalizing and retaining FAM-iRGD. Representative images from three independently studied tumors at each time point are shown. Scale bars, 50 μ m.

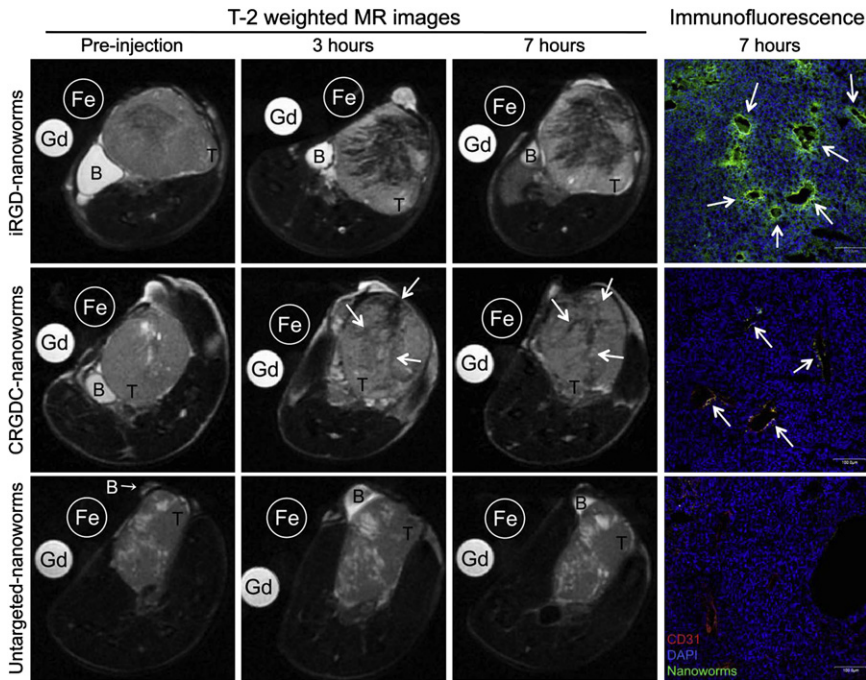


Figure 7. Tumor Imaging with iRGD-Coated Iron Oxide Nanoworms

T2-weighted magnetic resonance images of mice bearing orthotopic 22Rv1 human prostate tumors. The mice were injected intravenously with iron oxide nanoworms coated with iRGD, CRGDC, or no peptide (5 mg/kg of iron). Shown are axial images through the tumors acquired by repeated imaging before the nanoworm injection (Preinjection) and 3 hr or 7 hr after the injection. The orientation of the tumors is slightly different between the time points because the mice were anesthetized for each scan and reintroduced in the MRI instrument. Gadolinium (Gd) was used as a reference for T1 and Feridex (Fe) for T2 imaging agents. Note the wide hypointensity areas indicating the spreading of iRGD nanoworms in the tumor interstitium. CRGDC nanoworms only decreased the intensity of tumor vessels, and the untargeted nanoworms gave no signal in the tumor. Arrows point to the vasculature. T, tumor; B, urinary bladder. The rightmost panels represent the nanoworm distribution in tumor tissue examined by confocal microscopy. Green, nanoworms; red, CD31; blue, DAPI. Scale bars, 100 μ m. The images are representative of multiple tumor mice; iRGD nanoworms, n = 5; CRGDC nanoworms, n = 3; untargeted nanoworms, n = 3.

abraxane (Figure 8A). CRGDC-abraxane concentration was only about 2-fold higher than that of nontargeted abraxane in the tumors. In line with these results, iRGD-abraxane treatment resulted in significant inhibition of tumor growth at a dose at which untargeted abraxane showed no significant effect (Figure 8B); the slight reduction in tumor growth in the CRGDC group was not statistically significant. Treatment with the iRGD peptide alone at a dose equivalent to its molar amount in iRGD-abraxane did not affect tumor growth, indicating that the effect of iRGD-abraxane was not due to the disruption of the integrin signaling by the

iRGD peptide. An additional treatment study in a subcutaneous 22Rv1 tumor model with time-dependent tumor volume measurements confirmed the treatment data obtained with the orthotopic tumors (Figure S13B). A similar biodistribution of the abraxane formulations was also observed in the subcutaneous and orthotopic tumors (Figure S13A).

We next tested the efficacy of iRGD-abraxane in a tumor model unrelated to 22Rv1. We chose orthotopic tumors generated with the BT474 human breast cancer cell line, which expresses both αv integrins and neuropilin-1 at the cell surface

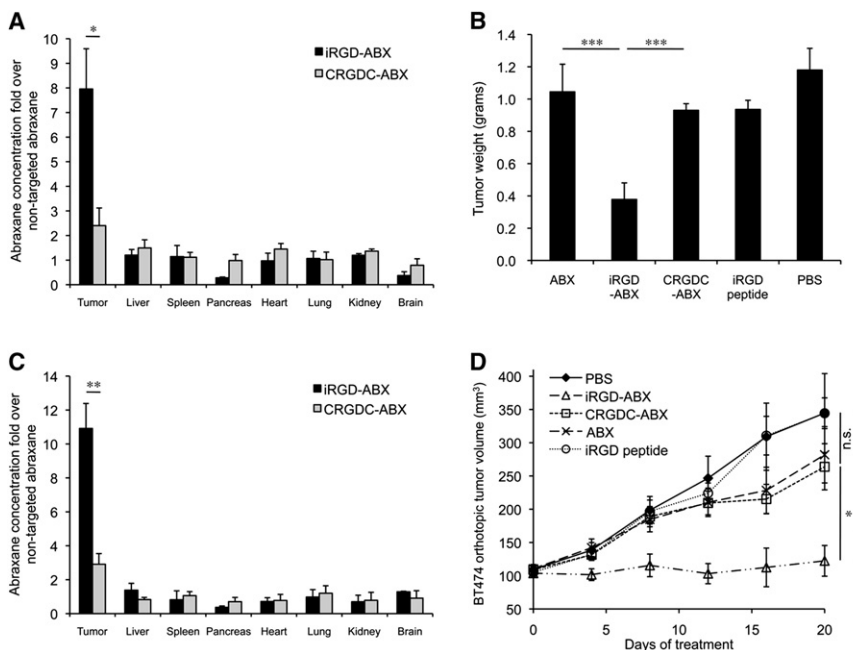


Figure 8. Tumor Treatment with iRGD-Coated Nanoparticles

(A and C) Abraxane quantification in orthotopic 22Rv1 (A) and BT474 (C) xenograft models. Abraxane was intravenously injected into tumor mice 3 hr earlier and captured from tumor extracts with a taxol antibody, followed by detection with a human albumin antibody. n = 3 for each group. (B and D) Long-term treatment of tumor mice with targeted abraxane conjugates. Mice bearing orthotopic 22Rv1 (B) or BT474 (D) xenografts were intravenously injected with peptide-coated abraxanes every other day at 3 mg paclitaxel/kg/injection. The treatment was continued for 14 days in (B) and 20 days in (D). (B) shows one of three experiments, which all gave similar results. The total number of mice in (B) was as follows: untargeted abraxane (ABX; n = 18), abraxane coated with CRGDC (CRGDC-ABX; n = 10) or iRGD (iRGD-ABX; n = 19), iRGD peptide alone as a control (iRGD peptide; n = 10), or PBS (n = 18). The number of mice per group was eight in (D). Statistical analyses were performed with Student's t test in (A) and (C) and ANOVA in (B) and (D). Error bars, SEM; n.s., not significant; *p < 0.05; **p < 0.01; ***p < 0.001.

(Figure S14). In addition, the BT474 cells are more resistant to abraxane (paclitaxel) than 22Rv1 as shown in cytotoxicity assays (Figure S15). When injected intravenously into the tumor mice, the iRGD-abraxane accumulated in the tumor 11-fold more than nontargeted abraxane and about 4-fold more than the CRGDC-abraxane (Figure 8C). Despite the resistance of the BT474 cells to paclitaxel, the iRGD-abraxane significantly inhibited the tumor growth in vivo (Figure 8D). The other abraxane formulations or iRGD peptide alone did not show significant effects at the same dose. Together, these results clearly demonstrate the efficacy of iRGD in drug delivery.

DISCUSSION

Our results delineate a technology to deliver diagnostics and therapeutics into the extravascular tumor parenchyma using a unique tumor-specific homing peptide, iRGD. The iRGD peptide follows a multistep tumor-targeting mechanism; the intact peptide binds to the surface of cells expressing αv integrins, where it is proteolytically cleaved to produce the CRGDK fragment. This fragment then binds to neuropilin-1 and penetrates tumor cells and tissues (schematized in Figure 4). Several pieces of data support the model. First, the affinity of iRGD for αv integrins is in the mid to low nanomolar range, similar to that of RGD peptides previously used in tumor targeting (Koivunen et al., 1993, 1995). Significantly, the proteolytically processed CRGDK fragment we identified within the targeted cells has lost most of its affinity to the integrins (about 50- to 150-fold reduction in affinity), which is in agreement with the observation that RGDK peptides lack cell attachment activity (Pierschbacher and Ruoslahti, 1984). Instead, the CRGDK fragment acquires an affinity for neuropilin-1 that is stronger than its residual affinity for αv integrins. These changes likely facilitate the transfer of CRGDK from integrins to neuropilin-1, and the resulting penetration activities. Each step in this multistep process evidently adds to the tumor specificity of iRGD. The expression of αv integrins is largely restricted to tumors (and other sites of angiogenesis or tissue repair), and neuropilin-1 is elevated in multiple tumor types (Eliceiri and Cheresch, 2001; Pellet-Many et al., 2008; Ruoslahti, 2002). The same may be true of the yet unknown processing protease(s). For example, matriptase, a membrane-bound protease, which preferentially cleaves proteins after a sequence similar to the R/KXXR/K CendR motif, is overexpressed in a number of tumor types (Uhland, 2006).

The initial recruitment of iRGD to cell surfaces appears to be crucial for its pronounced tumor targeting ability, since the related but non-integrin-binding peptide iRGE showed only modest uptake into cultured cells and was inefficient in targeting tumors in vivo. The presence of the tumor-specific recruitment element RGD distinguishes iRGD from some previously described tumor-targeting peptides. Jiang et al. (2004) have described a design for tumor-homing peptides in which a cationic cell-penetrating peptide is tethered to a negatively charged sequence that blocks the cell-penetrating activity. The tether contains a recognition sequence for a protease known to be elevated in tumors. These authors achieved a 3-fold increase in tumor homing. The greater homing we achieved with iRGD (12-fold over a control peptide) is likely due to the RGD-directed specific homing of the intact peptide. In addition,

the recruitment of iRGD to the cell surface through the RGD-integrin interaction is probably needed for the proteolytic cleavage that triggers the subsequent tumor penetration, as protease inhibitors are generally inactive on cell surfaces, but block proteolysis elsewhere (Hall et al., 1991). The unbiased screening we performed in identifying iRGD may also have selected for a protease that is more readily available to cleave an incoming peptide than the proteases with known expression but unknown availability in tumors.

Integrins shuttle between the cell surface and intracellular compartments (Pellinen and Ivaska, 2006). Certain viral pathogens take advantage of this mechanism in entering cells (Pellinen and Ivaska, 2006). However, as shown by our results, the cell-penetrating activity of iRGD is far greater than that of conventional RGD peptides. It far exceeds what can be accomplished with conventional RGD peptides and their mimics, which only take payloads to tumor vessels (this study; Murphy et al., 2008; Pasqualini et al., 1997). The strong tumor MRI signals provided by iRGD-coated iron oxide nanoworms and the enhanced tumor growth suppression by iRGD-linked abraxane demonstrate the potential of this peptide in tumor targeting.

The molecular mechanism of the rapid tumor tissue penetration of iRGD remains to be elucidated. However, several lines of evidence suggest that it may involve the so-called vascular permeabilization in the tumor induced by the CendR property of iRGD. Molecules such as vascular endothelial growth factor-165 and some semaphorins that have exposed CendR motifs increase vascular permeability (Jia et al., 2006; Acevedo et al., 2008). In addition, we have recently demonstrated that a prototypic CendR peptide, RPARPAR, induces vascular permeability (Teesalu et al., 2009). Some previously described tumor-specific cell-penetrating peptides that contain cryptic CendR sequences may share the same CendR-dependent tissue penetration mechanism (Hoffman et al., 2003; Joyce et al., 2003; Laakkonen et al., 2002; Porkka et al., 2002). For example, LyP-1 (CGNKRTRGC; Laakkonen et al., 2002), a cyclic peptide with a binding site for a specific receptor (Fogal et al., 2008), contains a cryptic CendR motif, KRTR. Like iRGD nanoparticles, LyP-1-coated nanoparticles extravasate into tumor tissue within minutes after an intravenous injection (Karmali et al., 2009; Laakkonen et al., 2002; von Maltzahn et al., 2008). CendR involvement in the activities of LyP-1 and other tumor-penetrating homing peptides remains to be studied, but seems likely. iRGD and the CendR system may help bring the “magic bullet” treatment of cancer closer to reality.

EXPERIMENTAL PROCEDURES

Tumor Models

Animal experimentation was performed according to procedures approved by the Animal Research Committees at the University of California, Santa Barbara, San Diego, and San Francisco, and the Burnham Institute for Medical Research. Xenografts were created by injecting nude mice with 10^6 human cancer cells orthotopically, subcutaneously, or into the tibia and the brain: prostate cancers PC-3 (Yang et al., 1999), PPC1 (Zhang et al., 2006), and 22Rv1 (Drake et al., 2005), pancreatic cancer MIA PaCa-2 (Sugahara et al., 2008), and breast cancer BT474 (Rusnak et al., 2001). Disseminated prostate tumors were generated by injecting 10^6 GFP-PC-3 cells (Yang et al., 1999) into the left ventricle of the heart of nude mice. Tumors were monitored with the X-ray system of the Image Station In Vivo FX (Eastman Kodak Company) or the Illumatool Bright Light System LT-9900 (Lighttools Research). Transgenic

mice were maintained as described previously (Arbeit et al., 1994; Hanahan, 1985; Hezel et al., 2006).

In Vivo Peptide and Phage Homing

Approximately 200 μg of FAM-labeled synthetic peptides (Karmali et al., 2009) were intravenously injected into tumor-bearing mice and allowed to circulate for 15 min to 2 hr. Tissues were collected and observed under UV light (Illuma-tool Bright Light System LT-9900) and processed for immunofluorescence (Karmali et al., 2009) or immunohistochemistry (Sugahara et al., 2008). To quantify the homing area of peptides within tumors, cryosections immunohistochemically stained with an anti-FITC antibody were scanned with the ScanScope CM-1 scanner and analyzed with the ImageScope software (Aperio Technologies; Fogal et al., 2008). To assess phage homing (Zhang et al., 2006), 10^8 plaque-forming units (pfu) of T7 phage were intravenously injected into tumor-bearing mice and allowed to circulate for 15 min. The mice were perfused through the heart with PBS containing 1% BSA and tissues were harvested for immunofluorescence. In some experiments, 50 μg of function-blocking anti-neuropilin-1 antibody (R&D Systems) or goat IgG (Abcam) was intravenously injected into the tumor mice 15 min prior to the phage injections. The phage were allowed to circulate for 10 min prior to perfusion and collection of the tumors and other tissues.

Preparation of Micelles

Lipids were purchased from Avanti Polar Lipids. DSPE-PEG_{2,000}-iRGD(FAM) was prepared by coupling FAM-iRGD peptide bearing a cysteine on its N terminus to 1,2-distearoyl-*sn*-glycero-3-phosphoethanolamine-N-maleimide(polyethylene glycol)_{2,000} (DSPE-PEG_{2,000}-maleimide) at 1:1 molar ratio at room temperature for 4 hr. DSPE-PEG_{2,000}-FAM was prepared by coupling 1,2-distearoyl-*sn*-glycero-3-phosphoethanolamine-N-amino(polyethylene glycol)_{2,000} (DSPE-PEG_{2,000}-amine) with NHS-fluorescein (Pierce Biotechnology) at a 1:1 molar ratio for 1 hr at room temperature. DSPE-PEG_{2,000}-Cy7 was prepared similarly using 1,2-distearoyl-*sn*-glycero-3-phosphoethanolamine-N-amino(polyethylene glycol)_{2,000} and Cy7-NHS ester (GE Healthcare).

DSPE-PEG_{2,000}-iRGD(FAM), DSPE-PEG_{2,000}-amine, and DSPE-PEG_{2,000}-Cy7 in 3:6:7:0.3 molar ratios were dissolved in chloroform/methanol (3:1, v/v). The solvent was evaporated and the dried lipid film was kept under vacuum for 8 hr and allowed to swell in PBS for 2 hr at 60°C. The vial was vortexed and sonicated to produce micelles. The micelles were sequentially filtered through 0.2 μm and 0.1 μm filters and washed with sterile PBS to remove unreacted peptides. Control Cy7 micelles were prepared using DSPE-PEG_{2,000}-FAM in place of DSPE-PEG_{2,000}-iRGD(FAM). The micelles were 15–25 nm in diameter as measured in deionized water by dynamic laser light scattering (refractive index, 1.59; viscosity, 0.89) on a Malvern Zetasizer Nano.

Optical In Vivo Imaging of Micelle-Peptide Conjugates

PDAC mice were injected with 100 μl of 1 mM micelles in PBS. After 3 hr, the mice were anesthetized, shaved, and subjected to whole-body imaging with the Odyssey Infrared Imaging System (LI-COR Biosciences).

Immunofluorescence

Tissue sections were processed as described previously (Karmali et al., 2009). Cells were grown on collagen I-coated coverslips (BD Biosciences) overnight and incubated with 10^8 pfu/ml of T7 phage for 30 min. The cells were fixed in 4% paraformaldehyde and stained with antibodies and DAPI (Molecular Probes). The primary antibodies were rat anti-mouse CD31 monoclonal antibody (BD Biosciences) and rabbit anti-human αv integrin (Chemicon), rabbit anti-human neuropilin-1 (Chemicon), mouse anti-human neuropilin-1 (Miltenyi Biotec), and rabbit anti-T7 phage (Teesalu et al., 2009) polyclonal antibodies. The secondary antibodies, Alexa 594 goat antibodies to mouse, rat, and rabbit IgG and Alexa 488 donkey anti-rabbit antibody, were from Molecular Probes. Cells and tissue sections were examined by a Fluoview 500 confocal microscope (Olympus America).

In Vitro Phage Binding and Penetration Assays

Suspended cells (10^6 cells in DMEM containing 1% BSA) were incubated with 10^8 pfu/ml of T7 phage for 1 hr at 4°C. The cells were washed four times with the binding buffer, lysed with lysis broth containing 1% NP-40, and titrated. Phage penetration assays used the same procedure, except that

the cells were incubated with phage at 37°C and that an acidic buffer (500 mM sodium chloride, 0.1 M glycine, and 1% BSA [pH 2.5]) was substituted for the binding buffer in the second wash to remove the phage that bound to the cell surface. Inhibitors of binding and penetration were added 20 min prior to incubation with phage. Noninfectious phage were prepared by treating phage with UV for 8 min in DMEM containing 1% BSA. The UV-inactivated phage particles expressing about 200 peptides per particle were used as multivalent inhibitors. Free synthetic peptides, mouse antibodies against human α1 , α2 , $\alpha\text{v}\beta\text{3}$, $\alpha\text{v}\beta\text{5}$, $\alpha\text{5}\beta\text{1}$, α4 , or αv integrins and integrin subunits (Chemicon), and goat anti-rat neuropilin-1 (R&D Systems) with mouse and goat IgG isotype controls (Abcam) were also tested. In some cases, 10^8 pfu phage were treated with 50 $\mu\text{g}/\text{ml}$ of crystalline trypsin for 5 min at 37°C before use. The proteolytic reaction was terminated with 5 mg/ml of soybean inhibitor.

Flow Cytometry

The experiments were performed as described previously (Sugahara et al., 2003) except that 1 mM of MgSO₄, CaCl₂, and MnCl₂ were added to the buffer containing the integrin antibodies. The antibodies were the same as in the cell binding assays and were detected with an Alexa 488 goat anti-mouse or goat anti-rabbit antibody (Molecular Probes). The cells were analyzed with an Easy-Cyte Plus System (Guava Technologies).

FAM-iRGD Fragment Isolation

PPC1 cells (10^7 cells in DMEM) were treated with 10 μM carbobenzoxy-leucyl-leucyl-leucinal (MG132; EMD Chemicals) for 30 min at 37°C to inhibit proteasomes and incubated with 20 μM of iRGD peptide labeled with FAM at the N or C terminus. The cells were washed once with acidic buffer and lysed in MPER (Pierce Biotechnology) containing protease inhibitors (Complete Mini EDTA-free; Roche Applied Science) on ice for 30 min. The sample was centrifuged for 30 min at 12,000 rpm. The supernatant was applied onto an anti-FITC affinity column and, after washing, bound peptides were eluted with glycine-HCl (pH 2.8). The eluate was subjected to mass spectrometry.

Affinity Measurements

Binding affinities of iRGD and CRGDK to $\alpha\text{v}\beta\text{3}$ and $\alpha\text{v}\beta\text{5}$ integrins (US Biological) and to neuropilin-1 (R&D Systems) were quantified by an ELISA by measuring IC₅₀. First, saturation binding assays were performed. Microtiter wells coated with 5 $\mu\text{g}/\text{ml}$ of the purified proteins were incubated for 1 hr at room temperature with various concentrations of biotinylated iRGD or CRGDK peptide in a HEPES-based buffer containing 1 mM of MgSO₄ and CaCl₂ for integrin binding and PBS for neuropilin-1 binding. After washing with the same buffer added with 0.01% Tween 20, streptavidin-conjugated horseradish peroxidase (Vector Laboratories) was added to the wells and incubated for 30 min at room temperature. Peptide binding was quantified with 2,2'-azino-bis(3-ethylbenzothiazoline-6-sulfonic acid) (Sigma-Aldrich) as a substrate. In subsequent competition studies, microtiter wells coated with the proteins were incubated with various concentrations of nonlabeled test peptides and a biotinylated reporter peptide at a concentration that gave half-maximal binding in the saturation binding assay. After 1 hr incubation at room temperature, the binding of the biotinylated peptide was quantified as above. Affinities were determined from the inhibition data as described previously (Müller, 1980).

Magnetic Resonance Imaging

Nude mice bearing 22Rv1 orthotopic human prostate tumors were injected intravenously with superparamagnetic iron oxide nanoworms (Park et al., 2009) coated with iRGD or CRGDK peptides or untargeted nanoworms at a dose of 5 mg/kg of iron. Each animal received nickel liposomes (0.2 μmol of Ni) intravenously 1 hr prior to the nanoworms to increase the half-life of the nanoworms (Simberg et al., 2007). The mice were repeatedly imaged before and 3 and 7 hr after injection of the nanoworms. For each scan, the mice were anesthetized with isoflurane and repositioned into a 30 mm diameter mouse coil. The axial plains were carefully matched to previous scans by measuring the height of the sections and comparing the vascular patterns in the images. Iron-sensitive MRI scans consisting of T2-weighted fast spin-echo were acquired using a 3-Tesla magnetic resonance imager (GE Healthcare). The conditions used were as follows: repetition time/echo time = 6.4 s/70 ms, echo train length = 32, readout bandwidth = ± 15.6 kHz, in-plane spatial resolution = 220 μm , field of view = (3.5 cm)², slice thickness = 1 mm,

number of excitation = 3. After imaging, tissues of interest were harvested without perfusion and processed for immunofluorescence.

Tumor Treatment Studies

Peptide-conjugated abraxanes were prepared and characterized as described previously (Karmali et al., 2009). For in vitro cytotoxicity studies, 22Rv1 or BT474 cells were seeded in 96 well culture plates (5×10^4 cells per well) and incubated overnight. The cells were incubated with various concentrations of the conjugates for 30 min at room temperature and washed with fresh culture media. MTT assays (Invitrogen) to assess cell viability were performed on the cells 48 hr later. For in vivo tumor treatment studies, nude mice bearing 2-week-old 22Rv1 orthotopic xenografts (typically about 250 mm^3 in tumor volume) were intravenously injected with the abraxane conjugates. The conjugates were given every other day for 14 days at a paclitaxel equivalent of 3 mg/kg/injection. The iRGD peptide control was administered in an equivalent amount of iRGD in each iRGD-abraxane dose. Mice bearing subcutaneous 22Rv1 tumors were treated similarly for 12 days, and orthotopic BT474 tumors for 20 days. The experiments were terminated according to the guidelines by the Animal Research Committee at the University of California, Santa Barbara. To study the homing pattern of the abraxane conjugates in the 22Rv1 orthotopic tumors, the conjugates were intravenously injected to tumor-bearing mice at a dose of 3 mg/kg and allowed to circulate for 3 hr. The mice were perfused through the heart and tissues of interest were harvested and processed for immunofluorescence.

Abraxane Quantification

Mice bearing 22Rv1 or BT474 tumors were intravenously injected with the abraxane conjugates at a paclitaxel equivalent of 9 mg/kg/injection. After 3 hr, the mice were perfused through the heart and tissues of interest were harvested. The tissues were homogenized in cold RIPA buffer (Pierce Biotechnology) containing protease inhibitors (Complete Mini EDTA-free) and kept on ice for 30 min. The samples were then centrifuged for 30 min at 14,000 rpm. The abraxane concentration in the supernatant was quantified with an ELISA: abraxane was captured with a taxol antibody (Novus Biologicals) coated onto a 96 well plate and detected with a human albumin antibody labeled with biotin (US Biological).

Statistical Analysis

Data were analyzed by two-tailed Student's t test and one-way analysis of variance (ANOVA), followed by suitable post-hoc test. The details are given in Table S3.

SUPPLEMENTAL DATA

Supplemental Data include 15 figures and three tables and can be found with this article online at [http://www.cell.com/cancer-cell/supplemental/S1535-6108\(09\)00382-1](http://www.cell.com/cancer-cell/supplemental/S1535-6108(09)00382-1).

ACKNOWLEDGMENTS

We thank M.J. Sailor and J.-H. Park for advice on the synthesis of iron oxide nanoworms, D.A. Cheresh for the M21 and R.M. Hoffman for the GFP-PC-3 cell lines, E. Engvall for comments on the manuscript, and L. Zhang and T. Järvinen for advice on the phage display screens. We also thank E. Allen and E. Drori for support with transgenic mice, J. Corbeil for help with MRI, and R. Varghese for editing. This work was supported by National Cancer Institute grants CA104898, CA115410, CA119414, CA119335, and CA30199 (Cancer Center Support Grant) and grants W81XWH-08-1-0727 and W81XWH-08-BCRP-CIA from the Department of Defense.

Received: April 23, 2009

Revised: September 22, 2009

Accepted: October 7, 2009

Published: December 7, 2009

REFERENCES

Acedo, L.M., Barillas, S., Weis, S.M., Göthert, J.R., and Cheresh, D.A. (2008). Semaphorin 3A suppresses VEGF-mediated angiogenesis yet acts as a vascular permeability factor. *Blood* 111, 2674–2680.

Arap, W., Pasqualini, R., and Ruoslahti, E. (1998). Cancer treatment by targeted drug delivery to tumor vasculature in a mouse model. *Science* 279, 377–380.

Arbeit, J.M., Münger, K., Howley, P.M., and Hanahan, D. (1994). Progressive squamous epithelial neoplasia in K14-human papillomavirus type 16 transgenic mice. *J. Virol.* 68, 4358–4368.

Arleth, L., Ashok, B., Onyuksel, H., Thiyagarajan, P., Jacob, J., and Hjelm, R.P. (2005). Detailed structure of hairy mixed micelles formed by phosphatidylcholine and PEGylated phospholipids in aqueous media. *Langmuir* 21, 3279–3290.

Cheresh, D.A., and Spiro, R.C. (1987). Biosynthetic and functional properties of an Arg-Gly-Asp-directed receptor involved in human melanoma cell attachment to vitronectin, fibrinogen, and von Willebrand factor. *J. Biol. Chem.* 262, 17703–17711.

Curnis, F., Gasparri, A., Sacchi, A., Longhi, R., and Corti, A. (2004). Coupling tumor necrosis factor- α with alphaV integrin ligands improves its antineoplastic activity. *Cancer Res.* 64, 565–571.

Drake, J.M., Gabriel, C.L., and Henry, M.D. (2005). Assessing tumor growth and distribution in a model of prostate cancer metastasis using bioluminescence imaging. *Clin. Exp. Metastasis* 22, 674–684.

Eliceiri, B.P., and Cheresh, D.A. (2001). Adhesion events in angiogenesis. *Curr. Opin. Cell Biol.* 13, 563–568.

Fogal, V., Zhang, L., Krajewski, S., and Ruoslahti, E. (2008). Mitochondrial/cell-surface protein p32/gC1qR as a molecular target in tumor cells and tumor stroma. *Cancer Res.* 68, 7210–7218.

Haley, B., and Frenkel, E. (2008). Nanoparticles for drug delivery in cancer treatment. *Urol. Oncol.* 26, 57–64.

Hall, S.W., Humphries, J.E., and Gonias, S.L. (1991). Inhibition of cell surface receptor-bound plasmin by α_2 -antiplasmin and α_2 -macroglobulin. *J. Biol. Chem.* 266, 12329–12366.

Hanahan, D. (1985). Heritable formation of pancreatic beta-cell tumours in transgenic mice expressing recombinant insulin/simian virus 40 oncogenes. *Nature* 315, 115–122.

Heldin, C.H., Rubin, K., Pietras, K., and Östman, A. (2004). High interstitial fluid pressure—an obstacle in cancer therapy. *Nat. Rev. Cancer* 4, 806–813.

Hezel, A.F., Kimmelman, A.C., Stanger, B.Z., Bardeesy, N., and Depinho, R.A. (2006). Genetics and biology of pancreatic ductal adenocarcinoma. *Genes Dev.* 20, 1218–1249.

Hoffman, J.A., Giraudo, E., Singh, M., Zhang, L., Inoue, M., Porkka, K., Hanahan, D., and Ruoslahti, E. (2003). Progressive vascular changes in a transgenic mouse model of squamous cell carcinoma. *Cancer Cell* 4, 383–391.

Jain, R.K. (1990). Vascular and interstitial barriers to delivery of therapeutic agents in tumors. *Cancer Metastasis Rev.* 9, 253–266.

Jia, H., Bagherzadeh, A., Hartzoulakis, B., Jarvis, A., Löhr, M., Shaikh, S., Aqil, R., Cheng, L., Tickner, M., Esposito, D., et al. (2006). Characterization of a bicyclic peptide neuropilin-1 (NP-1) antagonist (EG3287) reveals importance of vascular endothelial growth factor exon 8 for NP-1 binding and role of NP-1 in KDR signaling. *J. Biol. Chem.* 281, 13493–13502.

Jiang, T., Olson, E.S., Nguyen, Q.T., Roy, M., Jennings, P.A., and Tsien, R.Y. (2004). Tumor imaging by means of proteolytic activation of cell-penetrating peptides. *Proc. Natl. Acad. Sci. USA* 101, 17867–17872.

Joyce, J.A., Laakkonen, P., Bernasconi, M., Bergers, G., Ruoslahti, E., and Hanahan, D. (2003). Stage-specific vascular markers revealed by phage display in a mouse model of pancreatic islet tumorigenesis. *Cancer Cell* 4, 393–403.

Karmali, P.P., Kotamraju, V.R., Kastantin, M., Black, M., Missirlis, D., Tirrell, M., and Ruoslahti, E. (2009). Targeting of albumin-embedded paclitaxel nanoparticles to tumors. *Nanomedicine* 5, 73–82.

Koivunen, E., Gay, D.A., and Ruoslahti, E. (1993). Selection of peptides binding to the alpha 5 beta 1 integrin from phage display library. *J. Biol. Chem.* 268, 20205–20210.

Koivunen, E., Wang, B., and Ruoslahti, E. (1995). Phage libraries displaying cyclic peptides with different ring sizes: ligand specificities of the RGD-directed integrins. *Biotechnology (NY)* 13, 265–270.

- Laakkonen, P., Porkka, K., Hoffman, J.A., and Ruoslahti, E. (2002). A tumor-homing peptide with a targeting specificity related to lymphatic vessels. *Nat. Med.* **8**, 751–755.
- Lambert, S., Bouttier, M., Vassy, R., Seigneuret, M., Petrow-Sadowski, C., Janvier, S., Heveker, N., Ruscetti, F.W., Perret, G., Jones, K.S., and Pique, C. (2009). HTLV-1 uses HSPG and neuropilin-1 for entry by molecular mimicry of VEGF165. *Blood* **113**, 5176–5185.
- McAteer, M.A., Sibson, N.R., von Zur Muhlen, C., Schneider, J.E., Lowe, A.S., Warrick, N., Channon, K.M., Anthony, D.C., and Choudhury, R.P. (2007). In vivo magnetic resonance imaging of acute brain inflammation using microparticles of iron oxide. *Nat. Med.* **13**, 1253–1258.
- Müller, R. (1980). Calculation of average antibody affinity in anti-hapten sera from data obtained by competitive radioimmunoassay. *J. Immunol. Methods* **34**, 345–352.
- Murphy, E.A., Majeti, B.K., Barnes, L.A., Makale, M., Weis, S.M., Lutu-Fuga, K., Wrasidlo, W., and Cheresch, D.A. (2008). Nanoparticle-mediated drug delivery to tumor vasculature suppresses metastasis. *Proc. Natl. Acad. Sci. USA* **105**, 9343–9348.
- Park, J.H., von Maltzahn, G., Zhang, L., Derfus, A.M., Simberg, D., Harris, T.J., Ruoslahti, E., Bhatia, S.N., and Sailor, M.J. (2009). Systematic surface engineering of magnetic nanoworms for in vivo tumor targeting. *Small* **5**, 694–700.
- Pasqualini, R., Koivunen, E., and Ruoslahti, E. (1997). Alpha v integrins as receptors for tumor targeting by circulating ligands. *Nat. Biotechnol.* **15**, 542–546.
- Pellet-Many, C., Frankel, P., Jia, H., and Zachary, I. (2008). Neuropilins: structure, function and role in disease. *Biochem. J.* **411**, 211–226.
- Pellinen, T., and Ivaska, J. (2006). Integrin traffic. *J. Cell Sci.* **119**, 3723–3731.
- Pierschbacher, M.D., and Ruoslahti, E. (1984). Cell attachment activity of fibronectin can be duplicated by small synthetic fragments of the molecule. *Nature* **309**, 30–33.
- Porkka, K., Laakkonen, P., Hoffman, J.A., Bernasconi, M., and Ruoslahti, E. (2002). A fragment of the HMGN2 protein homes to the nuclei of tumor cells and tumor endothelial cells in vivo. *Proc. Natl. Acad. Sci. USA* **99**, 7444–7449.
- Ruoslahti, E. (2002). Specialization of tumour vasculature. *Nat. Rev. Cancer* **2**, 83–90.
- Ruoslahti, E. (2003). The RGD story: a personal account. *Matrix Biol.* **22**, 459–465.
- Ruoslahti, E., and Rajotte, D. (2000). An address system in the vasculature of normal tissues and tumors. *Annu. Rev. Immunol.* **18**, 813–827.
- Rusnak, D.W., Lackey, K., Affleck, K., Wood, E.R., Alligood, K.J., Rhodes, N., Keith, B.R., Murray, D.M., Knight, W.B., Mullin, R.J., and Gilmer, T.M. (2001). The effects of the novel, reversible epidermal growth factor receptor/ErbB-2 tyrosine kinase inhibitor, GW2016, on the growth of human normal and tumor-derived cell lines in vitro and in vivo. *Mol. Cancer Ther.* **1**, 85–94.
- Simberg, D., Duza, T., Park, J.H., Essler, M., Pilch, J., Zhang, L., Derfus, A.M., Yang, M., Hoffman, R.M., Bhatia, S., et al. (2007). Biomimetic amplification of nanoparticle homing to tumors. *Proc. Natl. Acad. Sci. USA* **104**, 932–936.
- Sipkins, D.A., Cheresch, D.A., Kazemi, M.R., Nevin, L.M., Bednarski, M.D., and Li, K.C. (1998). Detection of tumor angiogenesis in vivo by alphaVbeta3-targeted magnetic resonance imaging. *Nat. Med.* **4**, 623–626.
- Soker, S., Takashima, S., Miao, H.Q., Neufeld, G., and Klagsbrun, M. (1998). Neuropilin-1 is expressed by endothelial and tumor cells as an isoform-specific receptor for vascular endothelial growth factor. *Cell* **92**, 735–745.
- Sokoloff, A.V., Bock, I., Zhang, G., Sebestyén, M.G., and Wolff, J.A. (2000). The interactions of peptides with the innate immune system studied with use of T7 phage peptide display. *Mol. Ther.* **2**, 131–139.
- Steinhauer, D.A. (1999). Role of hemagglutinin cleavage for the pathogenicity of influenza virus. *Virology* **258**, 1–20.
- Sugahara, K.N., Murai, T., Nishinakamura, H., Kawashima, H., Saya, H., and Miyasaka, M. (2003). Hyaluronan oligosaccharides induce CD44 cleavage and promote cell migration in CD44-expressing tumor cells. *J. Biol. Chem.* **278**, 32259–32265.
- Sugahara, K.N., Hirata, T., Tanaka, T., Ogino, S., Takeda, M., Terasawa, H., Shimada, I., Tamura, J., ten Dam, G.B., van Kuppevelt, T.H., and Miyasaka, M. (2008). Chondroitin sulfate E fragments enhance CD44 cleavage and CD44-dependent motility in tumor cells. *Cancer Res.* **68**, 7191–7199.
- Teesalu, T., Sugahara, K.N., Kotamraju, V.R., and Ruoslahti, E. (2009). C-end rule peptides mediate neuropilin-1-dependent cell, vascular, and tissue penetration. *Proc. Natl. Acad. Sci. USA* **106**, 16157–16162.
- Uhland, K. (2006). Matriptase and its putative role in cancer. *Cell. Mol. Life Sci.* **63**, 2968–2978.
- von Maltzahn, G., Ren, Y., Park, J.H., Min, D.H., Kotamraju, V.R., Jayakumar, J., Fogal, V., Sailor, M.J., Ruoslahti, E., and Bhatia, S.N. (2008). In vivo tumor cell targeting with “click” nanoparticles. *Bioconjug. Chem.* **19**, 1570–1578.
- Wickham, T.J. (2000). Targeting adenovirus. *Gene Ther.* **7**, 110–114.
- Yang, M., Jiang, P., Sun, F.X., Hasegawa, S., Baranov, E., Chishima, T., Shimada, H., Moossa, A.R., and Hoffman, R.M. (1999). A fluorescent orthotopic bone metastasis model of human prostate cancer. *Cancer Res.* **59**, 781–786.
- Zhang, L., Giraudo, E., Hoffman, J.A., Hanahan, D., and Ruoslahti, E. (2006). Lymphatic zip codes in premalignant lesions and tumors. *Cancer Res.* **66**, 5696–5706.